ORGANOMETALLICS
Article

Organometallics **XXXX,** *XXX,* 000–000 A
DOI: 10.1021/om900498m

Infrared Spectra of Small Insertion and Methylidene Complexes in Reactions of Laser-Ablated Nickel Atoms with Halomethanes

Han-Gook Cho,[†] Lester Andrews,*[,‡] Bess Vlaisavljevich,[§] and Laura Gagliardi[§,⊥]

[†]*Department of Chemistry, University of Incheon, 177 Dohwa-dong, Nam-ku, Incheon, 402-749, South Korea,* [‡]*Department of Chemistry, University of Virginia, P.O. Box 400319, Charlottesville, Virginia 22904-4319,* [§]*Department of Chemistry, University of Minnesota, 207 Pleasant St. SE, Minneapolis, Minnesota 55455-0431, and* [⊥]*Department of Physical Chemistry, University of Geneva, 30, q. E. Ansermet, 1211 Genève, Switzerland*

Received June 12, 2009

Nickel carbene complexes, $CX_2{=}NiX_2$, are prepared along with the insertion products, $CX_3{-}NiX$, in reactions of laser-ablated Ni atoms with tetrahalomethanes. These reaction products are identified from matrix infrared spectra and density functional frequency calculations. In agreement with the previously studied Pt cases, the carbon−nickel bonds of the Ni carbene complexes are essentially double bonds with CASPT2-computed effective bond orders of 1.8−1.9. On the other hand, only insertion complexes are generated from dihalomethane and trihalomethane precursors. The nickel carbenes have staggered structures, and several insertion complexes containing C−Cl bonds reveal distinct bridged structures similar to those observed in the corresponding Fe products, which indicate effective coordination of Cl to the metal center. The unique F-bridged $CH_2F{-}NiCl$ structure is also observed.

Introduction

High oxidation-state complexes, first introduced in the 1970s,[1] are now considered an essential part of coordination chemistry and help to understand the nature of carbon−metal bonds.[2] Their rich chemistry includes growing applications in numerous syntheses including metathesis, catalytic properties, and C−H insertion.[3] Their distinct structures and photochemical properties have also provided testing grounds for theoretical applications.[4]

Recently small high-oxidation-state complexes have been reported from reactions of group 3−8 transition metals and actinides with small alkanes and halomethanes via C−H(X) insertion following H(X) migration.[5−9] These complexes also show distinct structures, particularly due to agostic interaction and dramatic photochemical reactions including photoreversibility. Their small sizes make them ideal for high-level theoretical approaches and, therefore, are considered as model systems for their much larger cousins. The higher oxidation-state complexes, however, are expected to be less favored on going far right among the transition metals in the periodic table because the d-orbital becomes more filled.

More recently small Pt carbene complexes, along with the insertion products, have been identified in reactions with methane and halomethanes.[10] The C−Pt bond orders computed by density functional theory and natural bond order range from 1.41 to 1.70 as Cl is replaced by F since the more electronegative halogen evidently supports a stronger carbon−metal bond. The small Pt methylidenes have a substantial amount of double bond character from $d_\pi{-}p_\pi$ bonding, and their C−Pt bonds are considerably shorter

*To whom correspondence should be addressed. E-mail: lsa@virginia.edu.

(1) (a) Fischer, E. O.; Kreis, G.; Kreiter, C. G.; Müller, J.; Huttner, G.; Lorenz, H. *Angew. Chem., Int. Ed. Engl.* **1973**, *12*, 564. (b) Schrock, R. R. *J. Am. Chem. Soc.* **1974**, *96*, 6796.

(2) (a) Herndon, J. W. *Coord. Chem. Rev.* **2009**, *253*, 1517. (b) Herndon, J. W. *Coord. Chem. Rev.* **2009**, *253*, 86. (c) Herndon, J. W. *Coord. Chem. Rev.* **2007**, *251*, 1158. (d) Herndon, J. W. *Coord. Chem. Rev.* **2006**, *250*, 1889. (e) Herndon, J. W. *Coord. Chem. Rev.* **2005**, *249*, 999. (f) Herndon, J. W. *Coord. Chem. Rev.* **2004**, *248*, 3, and earlier review articles in this series.

(3) (a) Crabtree, R. H. *Chem. Rev.* **1995**, *95*, 987, and references therein. (b) Wada, K.; Craig, B.; Pamplin, C. B.; Legzdins, P; Patrick, B. O.; Tsyba, I.; Bau, R. *J. Am. Chem. Soc.* **2003**, *125*, 7035. (c) Ujaque, G.; Cooper, A. C.; Maseras, F.; Eisenstein, O.; Caulton, K. G. *J. Am. Chem. Soc.* **1998**, *120*, 361.

(4) Clot, E.; Eisenstein, O. In *Computational Inorganic Chemistry*; Kaltzoyannis, N., McGrady, J. E., Eds.; *Structure and Bonding*; Springer: Heidelberg, 2004; pp 1−36. Aubert, C.; Buisine, O.; Malacria, M. *Chem. Rev.* **2002**, *102*, 813, and references therein.

(5) (a) Andrews, L.; Cho, H.-G. *Organometallics* **2006**, *25*, 4040, and references therein (review article, groups 4−6). (b) Lyon, J. T.; Cho, H.-G.; Andrews, L. *Organometallics* **2007**, *26*, 2519 (Ti, Zr, Hf + CHX_3, CX_4). (c) Lyon, J. T.; Cho, H.-G.; Andrews, L. *Organometallics* **2007**, *26*, 6373 (Cr, Mo, W + CHX_3, CX_4).

(6) (a) Cho, H.-G.; Andrews, L. *J. Phys. Chem. A* **2007**, *111*, 2480. (b) Cho, H.-G.; Andrews, L. *Organometallics* **2007**, *26*, 633. (Group 3).

(7) (a) Cho, H.-G.; Andrews, L. *Organometallics* **2007**, *26*, 4096. (b) Cho, H.-G.; Andrews, L. *Inorg. Chem.* **2008**, *47*, 1653. (Re).

(8) (a) Cho, H.-G.; Lyon, J. T.; Andrews, L. *Organometallics* **2008**, *27*, 5241. (b) Cho, H.-G.; Andrews, L. *Eur. J. Inorg. Chem.* **2008**, 2537. (c) Cho, H.-G.; Andrews, L. *Organometallics* **2008**, *27*, 1786. (Group 8).

(9) (a) Andrews, L.; Cho, H.-G. *J. Phys. Chem. A* **2005**, *109*, 6796. (b) Cho, H.-G.; Lyon, J. T.; Andrews, L. *J. Phys. Chem. A* **2008**, *112*, 6902. (c) Lyon, J. T.; Cho, H.-G.; Andrews, L. *Eur. J. Inorg. Chem.* **2008**, 1047 (Actinides).

(10) (a) Cho, H.-G.; Andrews, L. *J. Am. Chem. Soc.* **2008**, *130*, 15836. (b) Cho, H.-G.; Andrews, L. *J. Phys. Chem. A* **2008**, *112*, 12293. (c) Cho, H.-G.; Andrews, L. *Organometallics*, **2009**, *28*, 1358. (Pt).

than those of typical Pt(II) carbene complexes, leading to a conclusion that the small Pt methylidene complexes have substantial Pt(IV) character.[11]

As a continuation of our investigation on the chemistry of small transition-metal high-oxidation-state complexes, we report reactions of Ni with halomethanes. In contrast to the case of Pt,[10] which is considered as the most effective C−H insertion agent among group 10 metals,[10,12] only tetrahalomethanes generate Ni methylidenes. Several insertion products have interesting structures, particularly due to intermolecular interaction between X bonded to C and the metal center.

Experimental and Computational Methods

Laser-ablated nickel atoms were reacted with CCl_4 (Fisher), $^{13}CCl_4$ (90% enriched, MSD Isotopes), $CFCl_3$, CF_2Cl_2 (Dupont), $CHCl_3$, CH_2Cl_2, CH_2FCl, CH_2F_2 (Dupont), $CDCl_3$, CD_2Cl_2 (MSD Isotopes), CD_2FCl, and CD_2F_2 (synthesized[13]) in excess argon during condensation at 10 K using a closed-cycle refrigerator (Air Products Displex). These methods have been described in detail in previous publications.[10,14] Reagent gas mixtures were in the range 0.2−1.0% in argon. The Nd:YAG laser fundamental (1064 nm, 10 Hz repetition rate, 10 ns pulse width) was focused on a rotating metal target (Ni, 99.99%, Johnson Matthey) using 5−10 mJ/pulse. After initial reaction, infrared spectra were recorded at 0.5 cm^{-1} resolution using a Nicolet 550 spectrometer with a Hg−Cd−Te range B detector. Then samples were irradiated for 20 min periods by a mercury arc street lamp (175 W) with the globe removed using a combination of optical filters or annealed to allow further reagent diffusion.

To provide support for the assignment of new experimental frequencies and to correlate with related works,[5−10] density functional theory (DFT) calculations were performed using the Gaussian 03 program system,[15] the B3LYP and BPW91 density functionals,[16,17] and the 6-311++G(3df,3pd) basis sets for C, F, Cl, and Ni atoms.[18] Geometries were fully relaxed during optimization,

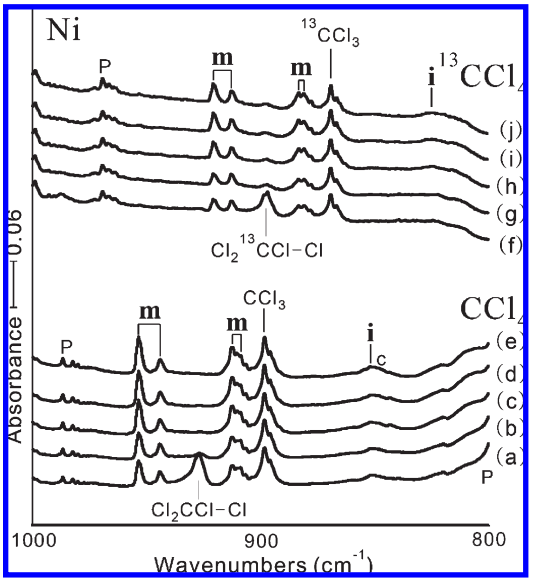

Figure 1. Infrared spectra in the 1000−800 cm^{-1} region for the reaction products of the laser-ablated nickel atom with CCl_4 isotopomers in excess argon at 10 K. (a) Ni and CCl_4 (0.5% in argon) co-deposited for 1 h. (b) As (a) after visible ($\lambda > 420$ nm) irradiation. (c) As (b) after ultraviolet (240−380 nm) irradiation. (d) As (c) after full arc ($\lambda > 220$ nm) irradiation. (e) As (d) after annealing to 26 K. (f) Ni and $^{13}CCl_4$ reagent (0.5% in argon) co-deposited for 1 h. (g−j) As (f) spectra taken following the same irradiation and annealing sequence. **i** and **m** designate the product absorption groups, while P and c stand for the precursor and common absorptions.

and the optimized geometry was confirmed by vibrational analysis. The vibrational frequencies were calculated analytically, and zero-point energy is included in the calculation of binding and reaction energies. Previous investigations have shown that DFT-calculated harmonic frequencies are usually slightly higher than observed frequencies,[5−10,19] and they provide useful predictions for infrared spectra of new molecules. Natural bond orbital (NBO) analysis[15,20] was done to help understand the carbon−nickel bonding in the carbenes, but the results were questionable, and the carbenes were examined using CASSCF/CASPT2 methods and triple-ζ (ANO-RCC-VTZP) basis sets.[21,22] An active space of (6,6) was chosen for the active orbitals involved in the C−M bond. A CASPT2 geometry optimization was performed for the carbenes starting from DFT geometries. The orbitals shown below and the occupation numbers used to compute the effective bond orders (EBO = bonding minus antibonding electons divided by two) are from the final calculation at the optimized geometry. A quadruple-ζ CASPT2 optimization was performed on $Cl_2Ni-CCl_2$ to confirm that the triple-ζ basis was sufficient.

Results and Discussion

Reactions of nickel atoms with halomethanes were investigated, and infrared spectra (Figures 1−6) and quantum

(11) Prokopchuk, E. M.; Puddephatt, R. J. *Organometallics* **2003**, *22*, 563, and references therein. Pt(IV).

(12) (a) Carroll, J. J.; Weisshaar, J. C.; Siegbahn, P. E. M.; Wittborn, C. A. M.; Blomberg, M. R. A. *J. Phys. Chem.* **1995**, *99*, 14388. (b) Low, J. J.; Goddard, W. A.III. *Organometallics* **1986**, *5*, 609. (c) Wang, X.; Andrews, L. *J. Phys. Chem. A* **2004**, *108*, 4838. (d) Cho, H.-G.; Andrews, L. *J. Phys. Chem. A* **2004**, *108*, 6272.

(13) Isotopic modifications synthesized: Andrews, L.; Willner, H.; Prochaska, F. T. *J. Fluorine Chem.* **1979**, *13*, 273.

(14) (a) Andrews, L.; Citra, A. *Chem. Rev.* **2002**, *102*, 885, and references therein. (b) Andrews, L. *Chem. Soc. Rev.* **2004**, *33*, 123, and references therein.

(15) Frisch, M. J.; Trucks, G. W.; Schlegel, H. B.; Scuseria, G. E.; Robb, M. A.; Cheeseman, J. R.; Montgomery, J. A., Jr.; Vreven, T.; Kudin, K. N.; Burant, J. C.; Millam, J. M.; Iyengar, S. S.; Tomasi, J.; Barone, V.; Mennucci, B.; Cossi, M.; Scalmani, G.; Rega, N.; Petersson, G. A.; Nakatsuji, H.; Hada, M.; Ehara, M.; Toyota, K.; Fukuda, R.; Hasegawa, J.; Ishida, M.; Nakajima, T.; Honda, Y.; Kitao, O.; Nakai, H.; Klene, M.; Li, X.; Knox, J. E.; Hratchian, H. P.; Cross, J. B.; Adamo, C.; Jaramillo, J.; Gomperts, R.; Stratmann, R. E.; Yazyev, O.; Austin, A. J.; Cammi, R.; Pomelli, C.; Ochterski, J. W.; Ayala, P. Y.; Morokuma, K.; Voth, G. A.; Salvador, P.; Dannenberg, J. J.; Zakrzewski, V. G.; Dapprich, S.; Daniels, A. D.; Strain, M. C.; Farkas, O.; Malick, D. K.; Rabuck, A. D.; Raghavachari, K.; Foresman, J. B.; Ortiz, J. V.; Cui, Q.; Baboul, A. G.; Clifford, S.; Cioslowski, J.; Stefanov, B. B.; Liu, G.; Liashenko, A.; Piskorz, P.; Komaromi, I.; Martin, R. L.; Fox, D. J.; Keith, T.; Al-Laham, M. A.; Peng, C. Y.; Nanayakkara, A.; Challacombe, M.; Gill, P. M. W.; Johnson, B.; Chen, W.; Wong, M. W.; Gonzalez, C.; Pople, J. A. *Gaussian 03, Revision C.02*; Gaussian, Inc.: Wallingford, CT, 2004.

(16) (a) Becke, A. D. *J. Chem. Phys.* **1993**, *98*, 5648. (b) Lee, C.; Yang, Y.; Parr, R. G. *Phys. Rev. B* **1988**, *37*, 785.

(17) (a) Becke, A. D. *Phys. Rev. A* **1988**, *38*, 3098. (b) Burke, K.; Perdew, J. P.; Wang, Y. In *Electronic Density Functional Theory: Recent Progress and New Directions*; Dobson, J. F., Vignale, G., Das, M. P. Ed.; Plenum, 1998.

(18) Raghavachari, K.; Trucks, G. W. *J. Chem. Phys.* **1989**, *91*, 1062.

(19) (a) Scott, A. P.; Radom, L. *J. Phys. Chem.* **1996**, *100*, 16502. (b) Andersson, M. P.; Uvdal, P. L. *J. Phys. Chem. A* **2005**, *109*, 3937.

(20) Reed, A. E.; Curtiss, L. A.; Weinhold, F. *Chem. Rev.* **1988**, *88*, 899.

(21) (a) Roos, B. O. The Complete Active Space Self-Consistent Field Method and its Applications in Electronic Structure Calculations. In *Advances in Chemical Physics; Ab Initio Methods in Quantum Chemistry−II*; Lawley, K. P., Ed.; John Wiley & Sons Ltd.: New York, 1987; Chapter 69, p 399. (b) Andersson, K.; Malmqvist, P.-Å.; Roos, B. O. *J. Chem. Phys.* **1992**, *96*, 1218 as implemented in Molcas 7.4.

(22) Roos, B. O.; Lindh, R.; Malmqvist, P.-Å.; Veryazov, V.; Widmark, P.-O. *J. Phys. Chem. A*, **2005**, *109*, 6575. (ANO-RCC-VTZP) basis.

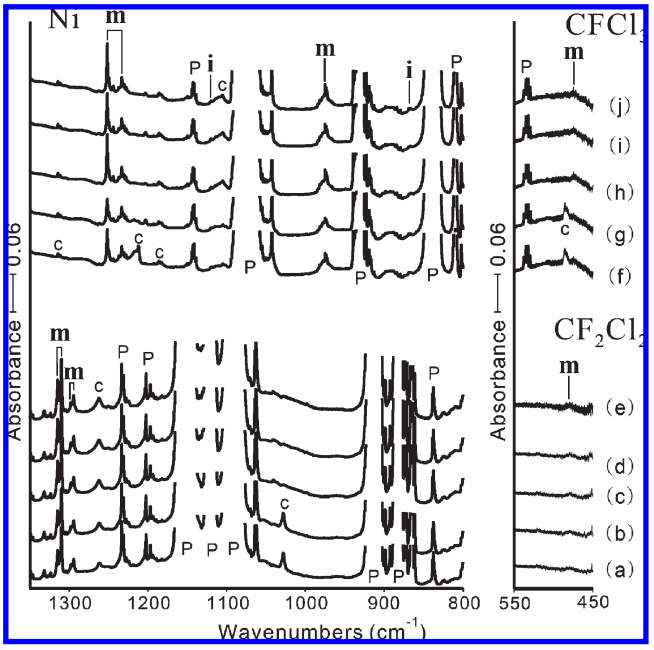

Figure 2. Infrared spectra in the 1350−800 and 550−450 cm^{-1} regions for the reaction products of the laser-ablated nickel atom with CF_2Cl_2 and $CFCl_3$ in excess argon at 10 K. (a) Ni and CF_2Cl_2 (0.5% in argon) co-deposited for 1 h. (b−e) As (a) spectra taken following the irradiation and annealing sequence described in Figure 1 caption (visible, UV, and full arc irradiations and annealing to 26 K). (f) Ni and $CFCl_3$ reagent (0.5% in argon) co-deposited for 1 h. (g−j) As (f) spectra taken following the same irradiation and annealing sequence. Notice the photoreversible intensity variation of the **m** absorptions in the $CFCl_3$ spectra (decrease and increase on visible and UV irradiations). **i** and **m** designate the product absorption groups, while P and c stand for the precursor and common absorptions.

chemical frequency calculations of the products and their structures (Figures 7, 8) will be presented in turn.

Ni + CX_4. Laser-ablated Ni atoms co-deposited with carbon tetrachloride in excess argon during condensation at 10 K produced two strong new absorptions at 953.3 cm^{-1} (944.0 cm^{-1} satellite for matrix site splitting) and 912.2 cm^{-1} (909.9 cm^{-1} shoulder for chlorine isotopic splitting) (labeled **m** for methylidene). Previously reported bands at 1036.4 cm^{-1} (CCl_3^+),[23] 1019.3 and 926.7 cm^{-1} ($Cl_2CCl-Cl$),[24] and 898 cm^{-1} (CCl_3)[25] were also observed: these are common to all laser-ablated metal experiments with CCl_4 as produced by ablation plume photolysis, and their identification follows from earlier work using vacuum ultraviolet irradiation.[23]

The product absorptions increased in concert 5, 20, and a few % on sequential irradiations in the visible ($\lambda > 420$ nm), ultraviolet (240−380 nm), and full arc ($\lambda > 220$ nm) regions, respectively. A similar experiment with $^{13}CCl_4$ (90% enriched) shifted the new absorptions to 920.5 cm^{-1} (912.6 cm^{-1} satellite) (12/13 isotopic frequency ratio of 1.0356) and to 883.2 cm^{-1} (880.8 cm^{-1} shoulder) (12/13 ratio of 1.0328). The appearance of a weak ^{12}C product band at 953.3 cm^{-1} with about 1/10 of the ^{13}C product band absorbance (Figure 1) confirms that a single carbon atom participates in these vibrational modes. The 909.9 and 880.8 cm^{-1} shoulders on the 912.2 and 883.2 cm^{-1} bands are 6/9 of the main band absorbances, which is appropriate for natural abundance chlorine isotopes in a species containing two equivalent chlorine atoms (statistical population of one ^{35}Cl and one ^{37}Cl vs two ^{35}Cl atoms).

(23) (a) Jacox, M. E.; Milligan, D. E. *J. Chem. Phys.* **1971**, *54*, 3935. (b) Jacox, M. E. *Chem. Phys.* **1976**, *12*, 51. (c) Prochaska, F. T.; Andrews, L. *J. Chem. Phys.* **1977**, *67*, 1091. (CCl_3^+)

(24) Maier, G.; Reisenauer, H. P.; Hu, J.; Hess, B. A., Jr.; Schaad, L. J. *Tetrahedron Lett.* **1989**, *30*, 4105. ($Cl_2CCl-Cl$).

(25) Andrews, L. *J. Chem. Phys.* **1968**, *48*, 972. (CCl_3).

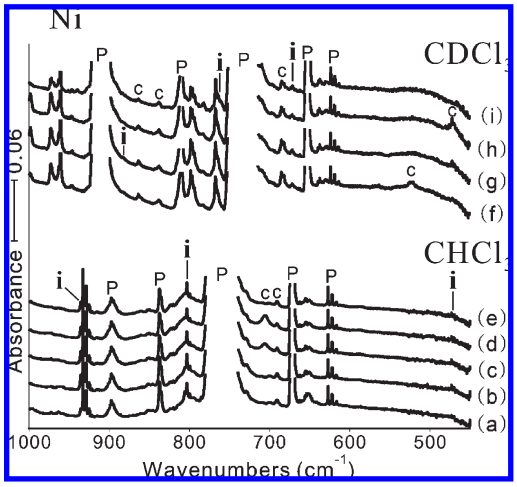

Figure 3. Infrared spectra in the 1000−450 cm^{-1} region for the reaction products of the laser-ablated nickel atom with $CHCl_3$ isotopomers in excess argon at 10 K. (a) Ni and $CHCl_3$ (0.5% in argon) co-deposited for 1 h. (b−e) As (a) spectra taken following the irradiation and annealing sequence described in Figure 1 caption (visible, UV, and full arc irradiations and annealing to 26 K). (f) Ni and $CDCl_3$ reagent (0.5% in argon) co-deposited for 1 h. (g−i) As (f) spectra taken following a sequence of visible and UV irradiation and annealing to 34 K. **i**, P, and c stand for product, precursor, and common absorptions, respectively.

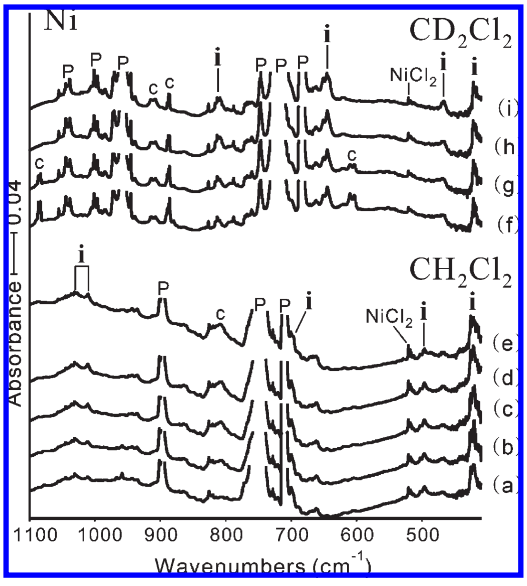

Figure 4. Infrared spectra in the 1100−410 cm^{-1} region for the reaction products of the laser-ablated nickel atom with CH_2Cl_2 isotopomers in excess argon at 10 K. (a) Ni and CH_2Cl_2 (0.5% in argon) co-deposited for 1 h. (b−e) As (a) spectra taken following the irradiation and annealing sequence described in Figure 1 caption (visible, UV, and full arc irradiations and annealing to 26 K). (f) Ni and CD_2Cl_2 reagent (0.5% in argon) co-deposited for 1 h. (g−i) As (f) spectra taken following a sequence of visible and UV irradiation and annealing to 28 K.

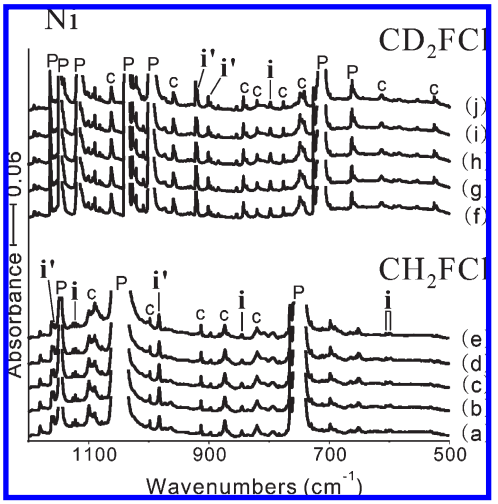

Figure 5. Infrared spectra in the 1200−500 cm^{-1} region for the reaction products of the laser-ablated nickel atom with CH_2FCl isotopomers in excess argon at 10 K. (a) Ni and CH_2FCl (0.5% in argon) co-deposited for 1 h. (b−e) As (a) spectra taken following the irradiation and annealing sequence described in Figure 1 caption (visible, UV, and full arc irradiations and annealing to 26 K). (f) Ni and CD_2FCl reagent (0.5% in argon) co-deposited for 1 h. (g−j) As (f) spectra taken following the same sequence. **i**, P, and c stand for product, precursor, and common absorptions, respectively.

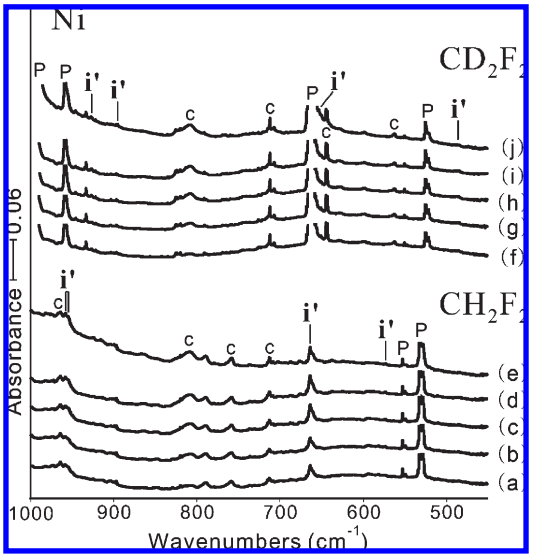

Figure 6. Infrared spectra in the 1000−450 cm^{-1} region for the reaction products of the laser-ablated nickel atom with CH_2F_2 isotopomers in excess argon at 10 K. (a) Ni and CH_2F_2 (0.5% in argon) co-deposited for 1 h. (b−e) As (a) spectra taken following the irradiation and annealing sequence described in Figure 1 caption (visible, UV, and full arc irradiations and annealing to 26 K). (f) Ni and CD_2F_2 reagent (0.5% in argon) co-deposited for 1 h. (g−j) As (f) spectra taken following the same sequence. **i**, P, and c stand for product, precursor, and common absorptions, respectively.

The two strong **m** product absorptions in the C−Cl stretching region suggest that a primary product with a CCl_2 moiety is generated during co-deposition of the laser-ablated nickel atoms and CCl_4. On the basis of our previous experience for reactions of metal atoms with hydrocarbons and halomethanes,[5−10] they are assigned to the symmetric and antisymmetric CCl_2 stretching modes of CCl_2−$NiCl_2$. The carbon 12/13 isotopic frequency ratio for a pure symmetric CCl_2 stretching mode is smaller than that for an antisymmetric stretching mode, but mixing with the Ni−C stretching mode increases the carbon participation and the 12/13 isotopic frequency ratio, as found for the CCl_2−$PtCl_2$ molecule.[10a] This mode is in fact C vibrating back and forth between Ni and two Cl atoms in an antisymmetric fashion. The totally symmetric counterpart calculated at 451.9 cm^{-1} (Table 1) has a very small carbon-13 shift, as

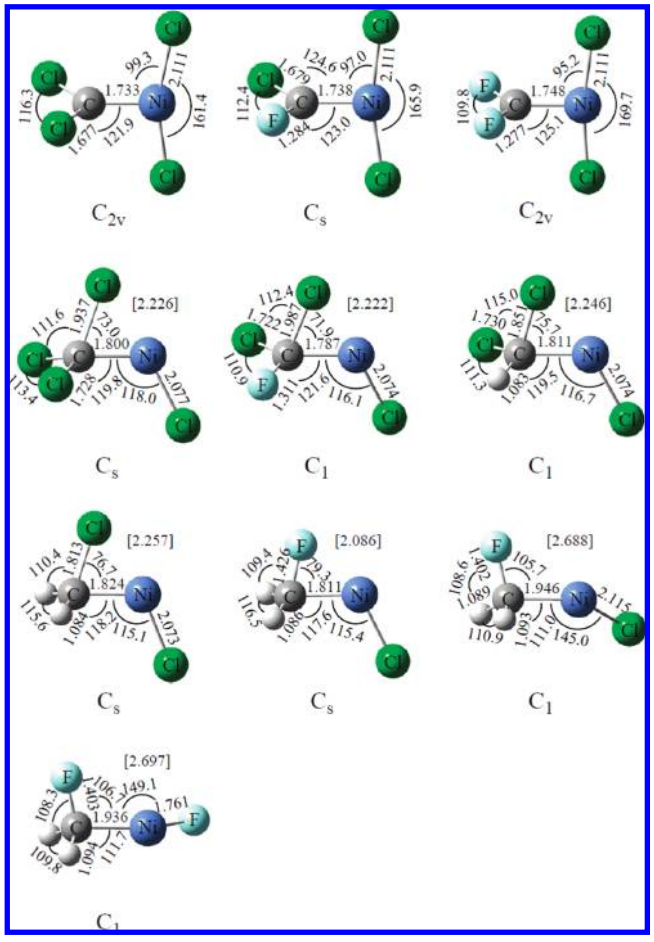

Figure 7. Structures calculated for the identified reaction products of nickel with halomethanes at the B3LYP level of theory using the 6-311++G(3df,3pd) basis sets for H, C, F, Cl, and Ni. Bond distances and angles are in Å and deg. Notice the staggered allene-type structures of the Ni methylidenes and the bridged structures of the insertion complexes [the bridged halogen−metal distance is given in brackets]. Molecular symmetries are given under each structure.

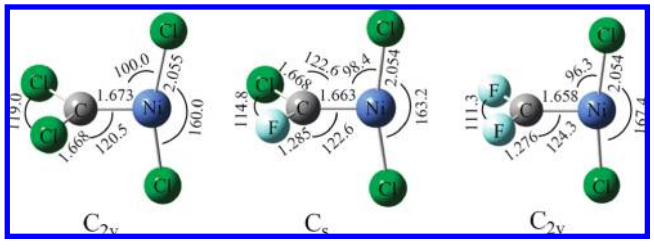

Figure 8. Calculated CASPT2 structures for the nickel carbenes.

Table 1. Observed and Calculated Fundamental Frequencies of CCl_2-NiCl_2 Isotopomers in the $^1A_1$ Ground State in C_{2v} Symmetry[a]

approximate description	$^{12}C^{35}Cl_2-Ni^{35}Cl_2$ obs[b]	B3LYP[c]	int[c]	BPW91[c]	int[c]	$^{13}C^{35}Cl_2-Ni^{35}Cl_2$ obs[b]	B3LYP[c]	int[c]	BPW91[c]	int[c]
A_1 C−Cl_2, Ni−C str.	953.3	945.2	248	958.2	196	920.5	912.7	231	925.0	182
B_2 CCl_2 str.	912.2	899.9	233	863.0	209	883.2	871.0	218	835.3	196
B_1 $NiCCl_2$ deform		452.4	6	453.7	7		431.8	24	410.2	2
A_1 Ni−C, C−Cl_2 str.		451.9	1	425.5	4		451.5	1	453.6	7
B_1 $NiCl_2$ str.		443.4	70	453.6	57		447.7	52	453.3	58
A_1 $NiCl_2$ str.		343.3	3	348.9	4		343.2	3	348.6	4
A_1 $NiCl_2$, CCl_2 bend		244.6	0	241.3	1		244.5	0	241.1	1
B_2 Cl_2NiCCl_2 def		194.9	0	191.4	0		194.3	0	190.8	0
B_2 $CNiCl_2$ def		106.6	4	103.5	2		106.5	4	103.4	2
A_1 $NiCl_2$ bend		92.1	3	96.5	0		92.0	3	96.4	0
B_1 $NiCl_2$ rock		57.6	1	69.1	1		57.6	1	69.1	1
A_2 CCl_2 twist		14.5	0	19.2	0		14.5	0	19.2	0

[a] Frequencies and intensities are in cm^{-1} and km/mol. Approximate mode descriptions as considerable mixing is involved. The first and fourth modes differ by phasing of the C motion, antisymmetric for the first and symmetric for the fourth mode. [b] Observed in an argon matrix. Chlorine isotopic splitting listed. [c] Harmonic frequencies and intensities computed with B3LYP or BPW91/6-311+G(3df).

Table 2. Observed and Calculated Fundamental Frequencies of CCl_3-NiCl Isotopomers in the ^1A Ground State[a]

approximate description	$^{12}CCl_3-NiCl$ obs[b]	B3LYP[c]	int[c]	$^{13}CCl_3-NiCl$ obs[b]	B3LYP[c]	int[c]
A′ CCl_2 s. str.	851.3	862.9	143	824.2	833.0	132
A″ CCl_2 as. str.	[d]	798.0	166	[d]	772.2	156
A′ $NiCCl_2$ deform		463.2	29		458.9	27
A′ C−Ni str.		432.0	110		426.9	96
A′ $NiCl_2$ as. str.		383.7	20		378.4	27
A′ $NiCl_2$ s. str.		290.4	5		290.3	4
A″ CCl_2 scis.		236.3	0		235.6	0
A′ Cl_2NiC deform		229.3	13		229.2	13
A′ $NiCl_2$ wag		165.4	33		164.8	33
A″ $NiCl_2$ bend		148.6	1		148.5	1
A″ $NiCl_2$ rock		78.2	2		78.2	2
A′ CCl_2 twist		76.4	4		76.4	4

[a] Frequencies and intensities are in cm^{-1} and km/mol. [b] Observed in an argon matrix. [c] Frequencies and intensities computed with B3LYP/6-311+G(3df) are for harmonic calculations. [d] Covered by precursor absorption. CCl_3-NiCl has a bridged C_s structure. Attempts to optimize with BPW91/6-311+G(3df) end up with the methylidene structure (CCl_2-NiCl_2).

the carbon atom hardly moves in this mode. The 912.2 cm^{-1} band is due to the antisymmetric C−Cl_2 stretching mode, and the 1.0328 isotopic 12/13 frequency ratio is virtually the same as found for the CCl_2-PtCl_2 molecule.[10a]

The observed CCl_2 stretching frequencies correlate well with the predicted values for CCl_2-NiCl_2 in its singlet ground state as shown in Table 1, and the carbon-13 isotopic shifts are also well reproduced (observed 32.8 and 29.0 cm^{-1} vs predicted 32.5 and 28.9 cm^{-1}). The observed frequencies are, however, slightly higher than the predicted values, and similar reversals are also observed from the C−X stretching frequencies in the previously studied halogenated late transition-metal carbene and carbynes.[8,10] The two strong observed (antisymmetric and symmetric) CCl_2 stretching absorptions and their ^{13}C counterparts are consistent with the DFT results and substantiate formation of the Ni methylidene, CCl_2-NiCl_2, via C−Cl bond insertion by Ni and subsequent Cl migration from C to Ni.

Unfortunately the weaker $NiCl_2$ antisymmetric stretching band is predicted too close to our observation limit, and all the other vibrational bands of the Ni methylidene are too weak to be observed (Table 1). It is also notable that the triplet state is energetically comparable (0.6 kcal/mol lower) to the singlet state; however, the CCl_2 frequencies calculated for the triplet state are much lower (e.g., the B3LYP frequencies of 862.5 and 839.9 cm^{-1} are 90.8 and 72.3 cm^{-1} lower than the observed values) and the predicted isotopic shifts (27.3 and 27.4 cm^{-1}) are not in good agreement as well. On the basis of the observed frequencies and their isotopic shifts, which are in excellent agreement with the predicted values, the Ni methylidene product has a singlet ground state.

Recently small Pt carbenes have been formed in reactions with methane and halomethanes and observed in the matrix infrared spectra. The C−Pt bond is clearly a double bond and apparently much stronger than those in larger Pt complexes.[10,11] Previous studies reveal that higher oxidation-state transition-metal complexes are favored on going down the family,[5−8,12] and therefore, Ni is normally considered a weaker C−H(X) insertion agent than Pt. Our identification of CCl_2-NiCl_2 from reactions of CCl_4 isotopomers, however, confirms that Ni also undergoes C−X insertion and following X migration from C to Ni.

Another weak product absorption marked "**i**" (**i** for insertion) is observed at 851.3 cm^{-1} and its ^{13}C counterpart at 824.2 cm^{-1} (12/13 ratio of 1.0329). They decrease slightly on visible irradiation, but increase slightly on UV irradiation. The frequency and ^{13}C shift indicate that it is a C−Cl stretching band of another product formed in the reaction of Ni and CCl_4. The previous studies[5−10] and computational results suggest that the most plausible product along with the methylidene complex is the insertion complex, CCl_3-NiCl. The insertion complex is expected to have a bridged structure (Figure 7) and to be energetically comparable to the methylidene complex (1.8 kcal/mol lower). The observed frequency and ^{13}C shift are in good agreement with the predicted values for the CCl_2 symmetric stretching mode of the insertion complex (862.9 and 27.1 cm^{-1}) as shown in Table 2. Unfortunately the antisymmetric CCl_2 stretching band and its ^{13}C counterpart are believed to be covered by precursor absorption, and other bands are calculated to be too weak to observe. We tentatively assign the weak **i** absorption to the CCl_2 symmetric stretching mode of the insertion complex in the singlet ground state. The singlet and triplet states are energetically close again (66.0 and 63.5 kcal/mol more stable than the reactants), but the triplet insertion complex would have the CCl_2 symmetric and strongest antisymmetric

Table 3. Observed and Calculated Fundamental Frequencies of CF_2-NiCl_2 and $CFCl-NiCl_2$ in the $^1A_2$ and $^1A''$ Ground States[a]

	CF_2-NiCl_2						$CFCl-NiCl_2$				
approximate description	obs[b]	B3LYP[c]	int[c]	BPW91[c]	int[c]	approximate description	obs[b]	B3LYP[c]	int[c]	BPW91[c]	int[c]
A_1 CF_2 s. str.	1310.0	1328.1	501	1279.1	528	A′ C−F str.	1251.9	1269.1	274	1207.6	283
B_2 CF_2 as. str.	1294.5	1302.8	242	1213.7	217.5	A′ C−Cl str.	974.8	966.2	363	946.1	295
A_1 CF_2 bend		726.4	15	705.7	4	A′ CFCl bend		540.3	2	538.7	6
B_1 CF_2 wag	520.8	579.5	59	546.7	24	A″ NiCFCl deform	474.5	508.1	25	480.2	7
B_1 $NiCl_2$ as. str.		451.9	69	453.9	55	A″ $NiCl_2$ as. str.		448.9	69	453.1	58
A_1 $NiCl_2$ s. str.		387.2	1	416.6	3	A′ C−Ni str.		360.8	3	372.2	5
A_1 C−Ni str.		334.6	0	336.3	0	A′ $NiCl_2$ s. str.		324.8	0	324.7	0
B_2 CF_2 rock		274.1	0	277.9	0	A′ CFCl rock		214.4	0	214.0	0
A_1 $NiCl_2$ bend		117.8	5	116.4	3	A′ $NiCl_2$ wag		112.5	4	111.1	2
B_2 $NiCl_2$ wag		88.4	7	93.4	2	A′ $NiCl_2$ bend		88.5	5	94.2	1
A_2 CCl_2 twist		21.4	2	56.9	1	A″ $NiCl_2$ rock		42.5	2	64.5	0
B_1 $NiCl_2$ rock		−8.0	0	−36.6	0	A″ CFCl twist		−9.5	0	−13.7	0

[a] Frequencies and intensities are in cm^{-1} and km/mol. [b] Observed in an argon matrix. [c] Frequencies and intensities computed with B3LYP or BPW91/6-311+G(3df) are for harmonic calculations. CF_2-NiCl_2 and $CFCl-NiCl_2$ have staggered allene-type C_{2v} and C_s structures.

Table 4. Observed and Calculated Fundamental Frequencies of $CFCl_2-NiCl$ in the ^1A Ground States[a]

	$CFCl_2-NiCl$				
approximate description	obs[b]	B3LYP[c]	int[c]	BPW91[c]	int[c]
C−F str.	1119.8	1181.0	225	1210.0	279
C−Cl str.	868.6, 866.5	892.9	242	945.3	294
CFCl bend		533.4	52	537.8	6
NiCFCl deform		474.6	93	479.8	6
$NiCl_2$ as. str.		441.0	53	453.7	59
C−Ni str.		330.2	6	371.6	6
$NiCl_2$ s. str.		291.0	10	325.1	0
CFCl rock		245.7	5	213.3	0
$NiCl_2$ wag		166.3	1	113.3	2
$NiCl_2$ bend		140.3	47	96.1	1
$NiCl_2$ rock		90.1	4	68.5	0
CFCl twist		77.2	4	19.0	0

[a] Frequencies and intensities are in cm^{-1} and km/mol. [b] Observed in an argon matrix. [c] Frequencies and intensities computed with B3LYP or BPW91/6-311+G(3df) are for harmonic calculations. $CFCl_2-NiCl$ has a bridged C_1 structure.

stretching band at ~790 and ~720 cm^{-1}, which are not observed from the spectra.

Ni + $CFCl_3$ and CF_2Cl_2. Infrared spectra from the reaction of Ni atoms with the chlorofluoromethanes are shown in Figure 2. In the $CFCl_3$ spectra three **m** absorptions are observed, which decrease one-third and double on visible and UV irradiations reversibly. The two strong product absorptions, one at 1251.9 cm^{-1} (with a satellite at 1244.3 cm^{-1}) in the C−F stretching region[26] and the other one at 974.8 cm^{-1} in the C−Cl stretching region, indicate that a primary product with a CFCl group is generated in the process of co-deposition and subsequent UV photolysis. It is most likely $CFCl-NiCl_2$, and the observed C−F and C−Cl stretching frequencies are well reproduced by computation as shown in Table 3. The weak absorption at 474.5 cm^{-1} is assigned to the NiCFCl deformation mode. All other bands are either too weak to observe or beyond our observation limit. The observed bands and good correlation with the predicted values support formation of the F-containing Ni methylidene.

Parallel to the Ni + CCl_4 case, weak **i** absorptions are also observed, which increase ~20% on UV photolysis. The one at 1119.8 cm^{-1} in the C−F stretching region is compared with the B3LYP frequency of 1181.0 cm^{-1} for the C−F stretching mode of the insertion complex, $CFCl_2-NiCl$ (Table 4). Another **i** absorption at 868.6 cm^{-1} (with a shoulder at 866.5 cm^{-1}) is assigned to the C−Cl stretching mode. The products from C−Cl insertion are much more stable than those via C−F insertion; $CFCl-NiCl_2$, $CCl_2-NiFCl$, $CFCl_2-NiCl$, and CCl_3-NiF are 63, 48, 62, and 49 kcal more stable than the reactants, respectively. $CFCl_2-NiCl$ has a C_1 structure with a bridging Cl atom similar to CCl_3-NiCl as shown in Figure 7.

Again the triplet states are energetically comparable; the singlet and triplet states for the Ni methylidenes are 63 and 64 kcal/mol more stable than the reactant ($Ni(^3F) + CFCl_3$). Optimization attempts for the triplet insertion complex also end up with the triplet methylidene. However, the triplet methylidene would have its C−Cl stretching and NiCFCl deformation bands at ~850 and ~410 cm^{-1}, which are not observed in this study. Most probably the F-containing Ni methylidene is in its singlet ground state (Table 3).

In the CF_2Cl_2 spectra the **m** absorptions remain unchanged on visible irradiation but increase ~15% and another ~5% on UV and full arc photolysis. The two strong **m** absorptions at 1310.0 cm^{-1} (with a satellite at 1315.1 cm^{-1}) and 1294.5 cm^{-1} (with a satellite at 1297.9 cm^{-1}) in the C−F stretching region[26] reflect formation of a primary product with a CF_2 group, most probably CF_2-NiCl_2. The observed CF_2 stretching bands are assigned to the symmetric and antisymmetric modes of the Ni methylidene, and the frequencies are well reproduced as shown in Table 3. A weak **m** absorption is also observed at 520.8 cm^{-1} and assigned to the CF_2 wagging mode. The tetrahalomethanes (CCl_4, $CFCl_3$, and CF_2Cl_2) used in this study all produce the Ni carbene complexes via C−Cl insertion following Cl migration from C to Ni. The observed vibrational characteristics show that CF_2-NiCl_2 is also in the singlet ground state because the triplet state would have the symmetric and antisymmetric CF_2 stretching bands at ~1250 and ~1200 cm^{-1} and the CF_2 wagging band at ~420 cm^{-1}, while the singlet and triplet states are 60 and 63 kcal/mol, respectively, more stable than the reactants.

No **i** absorption is observed in the CF_2Cl_2 spectra, unlike the CCl_4 and $CFCl_3$ cases. It is, however, in line with the fact that attempts to optimize the structure of the insertion complex all end up with that of CF_2-NiCl_2, suggesting that the original C−Cl bond insertion directly leads to Cl migration from C to Ni to form the methylidene complex in reaction of Ni with CF_2Cl_2. The products with Ni−Cl bonds

(26) Pavia, D. L.; Lampman, G. M.; George, S. K. *Introduction to Spectroscopy*, 3rd ed.; Brooks Cole: New York, 2000.

Table 5. Calculated Fundamental Frequencies of $CHCl_2$−NiCl Isotopomers in the $^1A'$ Ground State[a]

approximate description	$CHCl_2$−NiCl obs[b]	B3LYP[c]	int[c]	BPW91[c]	int[c]	$CDCl_2$−NiCl obs[b]	B3LYP[c]	int[c]	BPW91[c]	int[c]
C−H str.		3162.8	3	3084.5	2		2327.2	2	2269.4	1
C−H ip. bend		1233.0	22	1180.5	20	882.3	931.9	90	892.1	111
C−H oop. bend	935.1	995.1	33	945.2	49	763.8	819.2	45	788.9	69
C−Cl str.	803.1	805.3	128	779.0	163	671.3	727.2	46	698.2	49
CNiCl s. str.		601.5	19	606.5	16		560.1	35	559.8	26
CNiCl as. str.	472.9	471.7	63	440.0	12		457.2	40	436.8	13
Ni−Cl str.	422	428.8	67	421.0	102	420	426.3	71	409.6	87
CClNi s. str.		290.3	2	285.9	2		288.9	2	284.7	2
CClNi as. str.		223.3	2	225.0	2		222.9	2	224.5	2
CNiCl ip. bend		186.8	6	179.2	5		185.0	5	177.6	4
Ni−Cl oop. bend		97.9	3	98.6	2		97.1	3	97.7	2
Ni−Cl ip. bend		77.9	3	76.0	3		77.8	3	75.9	3

[a] Frequencies and intensities are in cm^{-1} and km/mol. [b] Observed in an argon matrix. [c] Frequencies and intensities computed with B3LYP or BPW91/6-311++G(3df, 3pd) are for harmonic calculations. $CHCl_2$−NiCl has a bridged C_1 structure.

Table 6. Observed and Calculated Fundamental Frequencies of CH_2Cl−NiCl Isotopomers in the ^1A Ground States[a]

approximate description	obs[b]	B3LYP[c]	int[c]	BPW91[c]	int[c]	CD_2Cl-NiCl obs[b]	B3LYP[c]	int[c]	BPW91[c]	int[c]
A″ CH_2 as. str.		3211.8	0	3136.9	0		2392.6	0	2337.5	0
A′ CH_2 s. str.		3106.3	2	3029.8	3		2246.4	2	2189.6	3
A′ CH_2 scis.		1426.3	2	1373.7	2		1059.5	4	1022.1	4
A′ CH_2 wag	1031.1	1080.8	11	1031.3	12	813.1	851.3	8	816.3	8
A″ CH_2 twist		988.8	0	946.9	0		728.2	0	700.2	0
A′ CClNi s. str.	700.0	696.0	28	709.7	24	645.0	639.8	39	648.2	33
A″ CH_2 rock		680.1	6	658.9	5		502.9	3	485.6	2
A′ CClNi as. str.	496.8	511.4	25	493.1	19	477.3	489.8	11	473.9	6
A′ NiCl str.	425	426.2	58	426.4	51	422	424.4	59	423.2	52
A′ CClNi bend		240.2	1	244.1	1		239.3	1	243.3	1
A″ CNiCl oop bend		104.4	3	103.6	1		103.1	3	102.6	1
A′ CNiCl ip bend		101.9	5	97.6	4		100.1	5	95.9	4

[a] Frequencies and intensities are in cm^{-1} and km/mol. [b] Observed (**i** absorption) in an argon matrix. [c] Frequencies and intensities computed with B3LYP or BPW91/6-311++G(3df, 3pd) are for harmonic calculations. CH_2Cl−NiCl has a bridged C_s structure in its triplet ground state.

are far more stable than those with Ni−F bonds. For example, CF_2−$NiCl_2$ and CFCl−NiFCl are 60 and 42 kcal/mol more stable than the reactants. It is consistent with the fact that the Ni−F stretching absorptions, which would be strong and near 650 cm^{-1}, are not observed in the $CFCl_3$ and CF_2Cl_2 spectra.

Ni + $CHCl_3$. Figure 3 shows the infrared spectra from reactions of Ni with $CHCl_3$ and $CDCl_3$, where the product absorptions are weaker relative to the tetrahalomethane cases. The product absorptions (all marked with "**i**") arise from the insertion complex, based on comparison with computed frequencies (Table 5). These bands increase ~50% on visible irradiation but decrease ~20 and ~10% on the following UV and full arc photolysis. The **i** absorption at 935.1 cm^{-1} and D counterpart at 793.6 cm^{-1} (H/D ratio of 1.178) are assigned to the C−H(C−D) out-of-plane bending mode. The relatively strong **i** absorption at 803.1 cm^{-1} has its D counterpart at 671.3 cm^{-1} (H/D ratio of 1.196) and is designated as the C−Cl stretching mode. The weak absorption at 472.9 cm^{-1} with its D counterpart at 450.1 cm^{-1} (H/D ratio of 1.051) is assigned to the CNiCl antisymmetric stretching mode. The one at 882.3 cm^{-1} from the deuterated product is assigned to the C−D in-plane bending mode, while its H counterpart expected at ~1180 cm^{-1} is probably covered by precursor absorption. The observed **i** absorptions substantiate formation of the Ni insertion complex in reaction with $CHCl_3$.

The absence of the **m** absorptions in the $CHCl_3$ spectra is in contrast to the tetrahalomethane cases, where the Ni methylidenes are the primary products. Chlorine migration from C to Ni in the insertion complex is evidently more difficult than the tetrahalomethane cases, and the insertion complex is also marginally more stable than the methylidene product: $CHCl_2$−NiCl and CHCl−$NiCl_2$ in their singlet ground states are 60 and 53 kcal/mol more stable than the reactants (Ni(^{3}F) + $CHCl_3$). Triplet $CHCl_2$−NiCl is again energetically comparable (2.6 kcal/mol higher) to the singlet insertion product, but its $CNiCl_2$ deformation bands would appear with similar intensities at ~720, ~520, and ~480 cm^{-1}, which are not observed in this study.

Ni + CH_2X_2. Figures 4−6 are the spectra from reactions of Ni with CH_2Cl_2, CH_2FCl, and CH_2F_2 and their deuterated isotopomers. Parallel to the $CHCl_3$ case, the insertion complexes are the primary products, and no **m** absorptions are observed, correlating well with the stability of the insertion complex relative to the carbene product in each case. CH_2Cl−NiCl(S), CH_2F−NiCl(T), and CH_2F−NiF(T) are 18, 2, and 11 kcal/mol more stable than the Ni carbene counterparts, respectively.

Figure 4 shows the product spectra from reactions of Ni and CH_2Cl_2 isotopomers, where the **i** absorptions remain unchanged on visible irradiation but increase ~5% on UV irradiation and increase slightly further on full arc photolysis. The insertion complex is believed to have a C_s structure with a bridging Cl atom (Figure 7), and the weakened C−Cl bond, due to coordination to the metal center, leads to a low

Table 7. Observed and Calculated Fundamental Frequencies of $CH_2F-NiCl$ Isotopomers in the ^1A Ground States[a]

	$CH_2F-NiCl$					$CD_2F-NiCl$				
approximate description	obs	B3LYP	int	BPW91	int	obs	B3LYP	int	BPW91	int
CH_2 as. str.		3197.3	1	3117.6	1		2384.1	1	2325.3	1
CH_2 s. str.		3086.0	6	3004.2	7		2229.9	5	2169.2	7
CH_2 scis.		1456.0	0	1402.8	0		1087.2	10	1049.1	9
CH_2 wag	1122.0	1177.2	29	1127.0	31	884.2	949.8	17	917.2	20
CH_2 twist		1137.1	3	1093.4	3		856.2	2	825.3	2
C−F str.	844.9	889.7	131	874.4	119	797.7	848.9	132	824.7	126
CH_2 rock		678.9	7	657.0	6		571.0	3	557.1	5
C−Ni str.	605.3, 598.4	629.8	12	614.2	20		501.4	4	485.0	3
Ni−Cl str.	425.3	434.0	44	435.2	31		433.4	44	434.7	31
NiCF bend		242.3	6	223.2	5		241.5	6	222.4	6
CH_2F tort		122.5	5	117.9	4		118.8	5	113.9	3
CNiCl bend		105.1	10	101.4	9		102.2	10	98.7	9

[a] Frequencies and intensities are in cm^{-1} and km/mol. [b] Observed (**i′** absorption) in an argon matrix. [c] Frequencies and intensities computed with B3LYP or BPW91/6-311++G(3df, 3pd) are for harmonic calculations. $CH_2F-NiCl$ has a bridged C_1 structure in its triplet ground state.

Table 8. Observed and Calculated Fundamental Frequencies of $CH_2F-NiCl$ Isotopomers in the ^3A Ground States[a]

	CH_2F-NiCl					$CD_2F-NiCl$				
approximate description	obs[b]	B3LYP[c]	int[c]	BPW91[c]	int[c]	obs[b]	B3LYP[c]	int[c]	BPW91[c]	int[c]
CH_2 as. str.		3110.7	9	3046.9	7		2308.4	5	2260.8	4
CH_2 s. str.		3022.1	13	2943.4	11		2188.1	9	2130.1	8
CH_2 scis.		1446.4	5	1391.1	3		1073.6	22	1036.2	33
CH_2 twist		1209.1	8	1167.1	3		901.1	2	872.0	2
CH_2 wag	1158.2	1207.1	70	1146.7	48	900.6	949.2	48	899.7	88
C−F str.	982.6	969.2	239	952.8	238	956.7	942.6	203	926.4	138
C−Ni str.		602.7	11	573.3	8		507.5	17	490.2	7
CH_2 rock		537.2	24	506.4	13		455.5	35	431.8	26
Ni−Cl str.		388.8	54	388.7	32		378.4	36	371.6	15
FCNi bend		164.9	6	176.0	3		163.2	6	173.5	3
CNiF bend		78.6	5	83.8	3		74.7	5	80.2	4
CH2F tort		30.1	8	39.6	5		29.5	8	38.6	5

[a] Frequencies and intensities are in cm^{-1} and km/mol. [b] Observed in an argon matrix. [c] Frequencies and intensities computed with B3LYP or BPW91/6-311++G(3df, 3pd) are for harmonic calculations. $CH_2F-NiCl$ has a bridged C_1 structure in its triplet ground state.

stretching frequency. The **i** absorption at 1031.1 cm^{-1} along with the D counterpart at 813.1 cm^{-1} (H/D ratio of 1.268) is assigned to the CH_2 wagging mode. Another one at 700.0 cm^{-1} shows a D shift of −55.0 cm^{-1} (H/D ratio of 1.085) and is assigned to the C−Cl···Ni symmetric stretching mode on the basis of the frequency and relatively small D shift. The one at 496.8 cm^{-1} has its D counterpart at 477.3 cm^{-1} (H/D ratio of 1.041) and is assigned to the C−Cl···Ni antisymmetric stretching mode. The strong absorption at 425 cm^{-1} near our observation limit shows its D counterpart at 422 cm^{-1} and is assigned to the Ni−Cl stretching mode. The four observed **i** absorptions and their D counterparts have good correlations with the DFT frequencies and substantiate formation of $CH_2Cl-NiCl$.

In addition, isolated $NiCl_2$ is observed at 520.9, 517.5, and 513.1 cm^{-1} (Figure 4) for chlorine and nickel isotopic splittings, in good agreement with previous observations.[27] Such $NiCl_2$ bands were detected with CCl_4 but not with $CHCl_3$. The observation of $NiCl_2$ suggests that CH_2-NiCl_2 may be formed in these experiments, but if so, it decomposes. The strong 425 cm^{-1} band is not appropriate for assignment to either singlet- or triplet-state carbene based on calculated frequencies.

The spectra from reactions of CH_2FCl and its deuterated isotopomer are shown in Figure 5, where **i** and **i′** absorptions are observed. The **i** absorptions remain unchanged upon visible and UV irradiation, but decrease ~20% on full arc irradiation, whereas the **i′** absorptions increase ~20% on visible irradiation, remain almost the same on UV irradiation, and decrease slightly on full arc irradiation. The observed frequencies are compared with the DFT frequencies in Tables 7 and 8. The **i** absorption at 1122.0 cm^{-1} along with its D counterpart at 884.2 cm^{-1} (H/D ratio of 1.268) is assigned to the CH_2 wagging mode of singlet $CH_2F-NiCl$ on the basis of the frequency and small D shift. The strong **i** absorption at 844.9 cm^{-1} has its D counterpart at 797.7 cm^{-1} (H/D ratio of 1.059) and is assigned to the C−F stretching mode of the bridged (C−F···Ni) complex in the singlet state (Figure 7). Another **i** absorption at 605.3 cm^{-1} (with a shoulder at 598.4 cm^{-1}) is assigned to the C−Ni stretching mode without observation of the D counterpart. The weak absorption at 425 cm^{-1} (not shown) is tentatively assigned to the Ni−Cl stretching mode. The observed absorptions all support formation of singlet, F-bridged $CH_2F-NiCl$ (Table 7). The strongest Ni−F stretching absorption for the Ni methylidene, $CH_2-NiFCl$, would be expected at ~650 cm^{-1} in both singlet and triplet states, which is not observed in this study.

The **i′** absorption at 1158.2 cm^{-1} has its D counterpart at 900.6 cm^{-1} (H/D ratio of 1.286), and we assign it to the CH_2 wagging mode of the insertion complex in the triplet state ($CH_2F-NiCl(T)$) on the basis of the frequency, H/D ratio,

(27) Jacox, M. E.; Milligan, D. E. *J. Chem. Phys.* **1969**, *51*, 4143. ($NiCl_2$).

and computational results. The strong **i′** absorption at 982.6 cm^{-1} with its D counterpart at 956.7 cm^{-1} (H/D ratio of 1.027) is assigned to the C−F stretching mode (Table 8). The structure of the insertion complex in the triplet state substantially differs from that in the singlet state, while the singlet and triplet states are almost isoergic (42 and 43 kcal lower than the reactants ($Ni(^3F) + CH_2FCl$)). Unlike the F-bridged structure in the singlet state, it does not bear a bridged structure and the C−Ni−Cl moiety is more linear (∠CNiCl = 145.0°), and therefore, the large structural difference is retained by trapping in the matrix and so is the electronic state. Unfortunately all other bands for $CH_2F-NiCl(T)$ are expected to be too weak to observe as shown in Table 8.

Figure 6 illustrates spectra from reaction of Ni with CH_2F_2 and CD_2F_2, where only one type of absorption marked "**i′**" is observed. The product absorptions decrease slightly on visible irradiation, increase ~30% on UV photolysis, and increase slightly further on full arc photolysis. We attribute these product absorptions to the insertion product in its triplet ground state (**i′** for triplet insertion complex). The **i′** absorption at 958.3 cm^{-1} (with a shoulder at 955.8 cm^{-1}) has its D counterpart at 927.1 cm^{-1} (H/D ratio of 1.034) and is assigned to the C−F stretching mode on the basis of the frequency and small D shift. The strong absorption at 663.7 cm^{-1} along with its D counterpart at 657.0 cm^{-1} (H/D ratio of 1.010) is assigned to the Ni−F stretching mode. The weaker **i′** absorption at 573.2 cm^{-1} has its D counterpart at 484.0 cm^{-1} (H/D ratio of 1.184) and is assigned to the CH_2 rocking mode. Another **i′** absorption is observed at 927.0 cm^{-1} in the CD_2F_2 spectra, and its H counterpart is believed covered by precursor absorption. It is assigned to the CH_2 wagging mode. The carbene complex (CH_2-NiF_2) is 15 and 11 kcal/mol higher in the singlet and triplet states than the insertion complex and would show the strong NiF_2 antisymmetric stretching band at ~750 cm^{-1}, which is not observed. The singlet insertion complex (4.5 kcal/mol higher than that in the triplet state) would have the strong C−F stretching band at ~830 cm^{-1} and its D counterpart at ~790 cm^{-1}, which are not observed in the spectra.

Structures of Ni Complexes. The calculated structures of the Ni complexes identified here are illustrated in Figure 7. The carbene complexes, CCl_2-NiCl_2, $CFCl-NiCl_2$, and CF_2-NiCl_2, have staggered structures, parallel to the corresponding group 8 metal and Pt complexes.[8,10] The B3LYP-computed C−Ni bond lengths of the small Ni carbenes of 1.733, 1.738, and 1.748 Å are slightly longer than CASPT2 values, 1.673, 1.663, and 1.658 Å, which may be compared with those of 1.83−1.92 Å for typical Ni carbenes.[28] The CASPT2 structures for the carbenes are shown in Figure 8.

New CASSCF/CASPT2 calculations were performed on the carbenes in order to characterize the nickel−carbon bonds. The molecular orbitals involved in the C−Ni bonds are illustrated in Figure 9. The EBO, effective bond orders (bonding minus antibonding occupancy divided by two), of CCl_2-NiCl_2, $CFCl-NiCl_2$, and CF_2-NiCl_2 are 1.81, 1.84, and 1.87 as shown. Analogous calculations reveal 1.89, 1.90, and 1.91 EBO values for the corresponding Pt complexes. In agreement with the previously characterized group 3−8 metal, actinide, and Pt carbenes,[5−10] the methylidene C−Ni bond is essentially a double bond. The increasing effective bond order with the number of F atoms is also observed in previously studied Pt systems,[10] suggesting that the more electronegative F substituent on carbon contracts the C 2p orbitals and thus enhances the C 2p-Ni 3d orbital overlap.

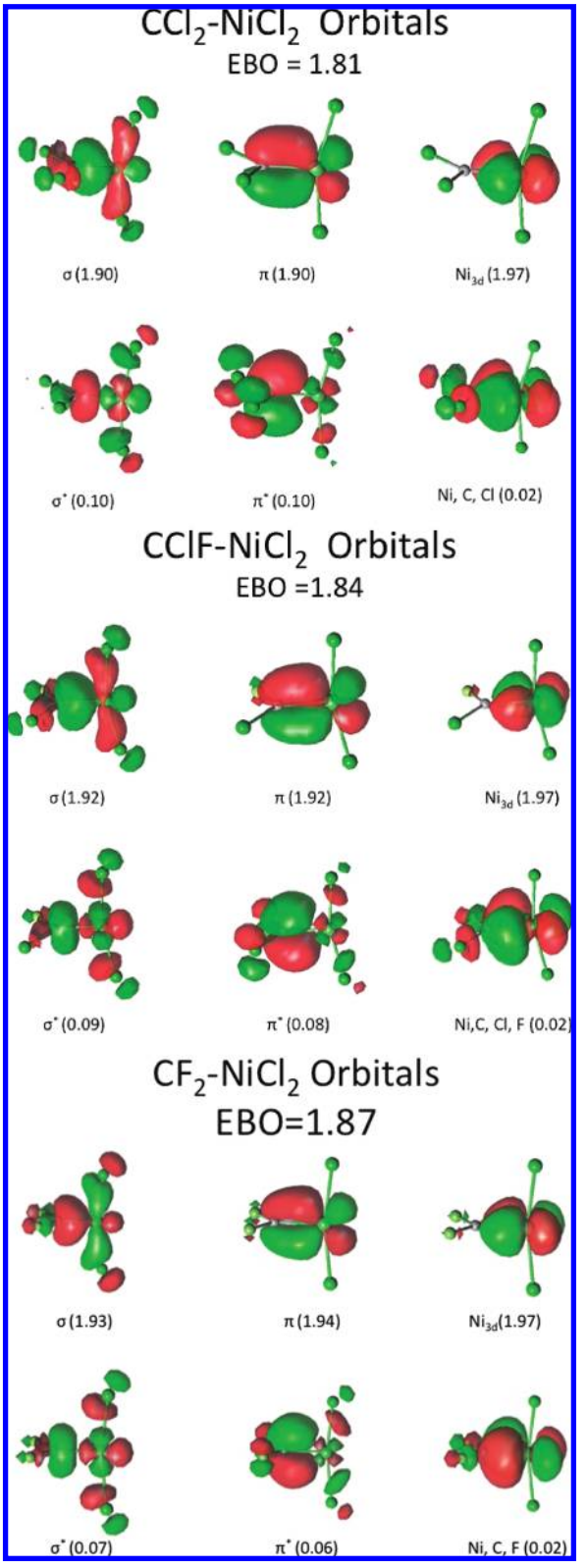

Figure 9. Calculated CASPT2 orbitals involved in the carbon−nickel double bonds. Occupation numbers given in parentheses.

(28) (a) Miki, K.; Taniguchi, H.; Kai, Y.; Kasai, N.; Nishiwaki, K.; Wada, M. *J. Chem. Soc., Chem. Commun.* **1982**, 1180. (b) Hou, H.; Gantzel, P. K.; Kubiak, C. P. *J. Am. Chem. Soc.* **2003**, *125*, 9564. (c) Normand, A. T.; Hawkes, K. J.; Clement, N. D.; Cavell, K. J.; Yates, B. F. *Organometallics* **2007**, *26*, 5352 (C−Ni length).

The Ni insertion complexes with X (particularly Cl) bonded to C have bridged structures as shown in Figure 7, and similar bridged structures (with bridging Cl) are observed in the Fe insertion complexes $CH_2Cl-FeCl$ and $CHCl_2-FeCl$.[8] Coordination of Cl electrons to the metal center is evidently more efficient than that of F, and $CH_2F-NiCl$ is believed to be the first F-bridged complex between C and M to the best of our knowledge. Coordination of F electrons to Ni is, however, not as effective as that of Cl; the ∠FCNi (79.3°) is larger than those of the Cl-bridging complexes (∠ClCNi = 71.9−76.7), and vibrational analysis shows that the contribution of the Ni···F stretching motion to the C−F stretching mode is insignificant.

As described above, the singlet and triplet states of the identified products except CH_2F-NiF are almost isoergic; however, the observed vibrational characteristics correlate with those predicted for the singlet states. In the case of $CH_2F-NiCl$, evidence shows that both the singlet and triplet states are trapped in a matrix as described above. It is not clear at the moment why the singlet Ni products are more favored in the matrix. The singlet Ni products are in line with the identified singlet Pt complexes.[10] Unlike the Ni cases, the singlet states of the Pt products are substantially more stable than the triplet states.

Reactions. Previous studies and the present results reveal that high-oxidation-state complexes are generated from reactions of group 3−10 transition metals and actinides with small alkanes and halomethanes.[5−10,29] However, the preference for methylidene products in reactions of group 10 metals varies substantially. Pt, which is regarded in general as the strongest insertion agent among group 10 metals,[12] forms carbenes not only with haloalkanes but with less reactive methane as well.[10] Analogous Ni carbene complexes are, on the other hand, far less favored. They are produced only in reactions with tetrahalomethanes, thanks to the preference for reaction of the M−X bond (particularly the M−Cl bond) over the M−H bond. Only the insertion complex is formed with chloroform and dihalomethane precursors. It is possible that repulsion between halogen atoms on the carbon center in the insertion product increases the rate of α−X transfer. Overall these results suggest that group 10 metals are near the limit of carbene complex formation in reactions with small alkanes and halomethanes, which is consistent with the fact that Ni carbene complexes are rare.[2] The observation of $NiCl_2$ in the CH_2Cl_2 experiments suggests that the CH_2-NiCl_2 carbene may be formed but decomposes.

Investigations in our laboratory have shown that laser-ablated transition-metal atoms react with halomethanes through C−X bond activation/insertion followed by α−X transfer,[8−10] reaction 1.

$$M^* + CX_4 \rightarrow CX_3-MX^* \rightarrow CX_2-MX_2^* \rightarrow CX-MX_3 \quad (1)$$

The present results reveal that C−X bond insertion by group 10 metal atoms occurs readily in reactions with halomethanes, and in the case of tetrahalomethanes, X migration from C to M also follows. However, further X migration to form the carbyne product has not been observed, probably due to the much higher energy of the product. For example, $CCl-PtCl_3$ is 27 kcal/mol higher in energy than $CCl_2{=}PtCl_2$,[10] and geometry optimization for $CCl-NiCl_3$ and $CCl-PdCl_3$ results in the corresponding carbene complexes.

Conclusions

Laser-ablated Ni atoms react with halomethanes, and the products are identified on the basis of isotopic shifts and correlation with the DFT results. The CX_2-NiX_2 molecules are produced by reactions with tetrahalomethanes, revealing that group 10 metals all form carbenes, while the reaction is more exothermic and the yield much higher for X = Cl than X = F, parallel to the previously studied Pt case.[10] On the other hand, only insertion complexes are identified from reactions with precursors containing H substituents, indicating that X migration from C to M following initial C−X bond insertion becomes much more difficult. This also suggests that group 10 metals are close to the limit where the carbene complex is no longer produced in transition-metal reactions with halomethanes. In agreement with the Pt case, the carbon−metal bonds of the Ni carbenes are essentially double bonds with effective bond orders in the range 1.8−1.9.

Although singlet states are clearly the most stable for the corresponding Pt complexes,[10] DFT calculations show that the singlet and triplet states are often nearly isoergic for the Ni complexes. However, the observed vibrational characteristics show that most of the Ni products also have singlet ground states. The identified Ni carbene complexes all have staggered structures, whereas the insertion products with a C−Cl bond have bridged structures, indicative of efficient Cl electron donation to the metal center. $CH_2F-NiCl$ reveals a unique F-bridged structure.

Acknowledgment. We gratefully acknowledge financial support from National Science Foundation (U.S.) Grant CHE 03-52487 to L.A., and support from Korea Institute of Science and Technology Information (KISTI) by Grant No. KSC-2008-S02-0001 and from the Swiss National Science Foundation (grant 200020-120007).

(29) Cho, H.-G.; Andrews, L. *Reactions of group 9 metals with halomethanes*, unpublished data.